Association Thermodynamics and Conformational Stability of β-Sheet Amyloid β(17-42) Oligomers: Effects of E22Q (Dutch) Mutation and Charge Neutralization

Nikolay Blinov,[†‡] Lyudmyla Dorosh,[†] David Wishart,[†§] and Andriy Kovalenko[†‡*]

[†]National Institute for Nanotechnology, National Research Council of Canada, Edmonton, Alberta, Canada; and [‡]Department of Mechanical Engineering and [§]Departments of Computing Science and Biological Sciences, University of Alberta, Edmonton, Alberta, Canada

ABSTRACT Amyloid fibrils are associated with many neurodegenerative diseases. It was found that amyloidogenic oligomers, not mature fibrils, are neurotoxic agents related to these diseases. Molecular mechanisms of infectivity, pathways of aggregation, and molecular structure of these oligomers remain elusive. Here, we use all-atom molecular dynamics, molecular mechanics combined with solvation analysis by statistical-mechanical, three-dimensional molecular theory of solvation (also known as 3D-RISM-KH) in a new MM-3D-RISM-KH method to study conformational stability, and association thermodynamics of small wild-type Aβ_{17-42} oligomers with different protonation states of Glu^{22}, as well the E22Q (Dutch) mutants. The association free energy of small β-sheet oligomers shows near-linear trend with the dimers being thermodynamically more stable relative to the larger constructs. The linear (within statistical uncertainty) dependence of the association free energy on complex size is a consequence of the unilateral stacking of monomers in the β-sheet oligomers. The charge reduction of the wild-type Aβ_{17-42} oligomers upon protonation of the solvent-exposed Glu^{22} at acidic conditions results in lowering the association free energy compared to the wild-type oligomers at neutral pH and the E22Q mutants. The neutralization of the peptides because of the E22Q mutation only marginally affects the association free energy, with the reduction of the direct electrostatic interactions mostly compensated by the unfavorable electrostatic solvation effects. For the wild-type oligomers at acidic conditions such compensation is not complete, and the electrostatic interactions, along with the gas-phase nonpolar energetic and the overall entropic effects, contribute to the lowering of the association free energy. The differences in the association thermodynamics between the wild-type Aβ_{17-42} oligomers at neutral pH and the Dutch mutants, on the one hand, and the Aβ_{17-42} oligomers with protonated Glu^{22} , on the other, may be explained by destabilization of the inter- and intrapeptide salt bridges between Asp^{23} and Lys^{28}. Peculiarities in the conformational stability and the association thermodynamics for the different models of the Aβ_{17-42} oligomers are rationalized based on the analysis of the local physical interactions and the microscopic solvation structure.

INTRODUCTION

Amyloid fibrils are associated with many neurodegenerative diseases, including Alzheimer's, Parkinson's, and prion diseases (1,2). Resolving the molecular structure and understanding the molecular mechanisms of formation of neurotoxic amyloidogenic oligomers and amyloid fibrils are crucial for earlier diagnostics and prevention of such diseases. It has been observed in the x-ray scattering experiments that amyloid fibrils are characterized by cross-β structural motif (3), but until recently, only low-resolution structures of fibrils were available. The studies on the yeast prion protein Sup35 (4) and short fragments of other proteins (5) unveiled a possible molecular structure of amyloid fibrils. The molecular models of amyloid (A)β fibril associated with Alzheimer's disease have been proposed based on solid-state nuclear magnetic resonance experiments (6,7) and hydrogen/deuterium-exchange nuclear magnetic resonance combined with mutagenesis studies (8).

Mechanisms of amyloidogenesis are well studied for a number of amyloidogenic proteins (1,9,10). Recently, direct experimental measurements of kinetic and thermodynamics of amyloid formation became possible (11). At the same time, the molecular details of the process of the fibril formation remain elusive. The experimental data suggest that there are two distinct stages in the fibril growth (1,12,13). At the first, nucleation stage, amorphous nontoxic aggregates could be formed. The aggregation of misfolded proteins also results in formation of globular oligomers (or protofibrils) (1), and they may transform into amyloid fibrils. These globular oligomers can be regarded as a precursor state for mature fibrils. Their molecular structure is unknown, but based on their toxicity and ability to seed fibrilization, it was suggested that there may be a similarity in the structure between some toxic oligomers and amyloid fibrils (14). The nucleation stage of amyloidogenesis is followed by the elongation stage, where the intermediate oligomeric aggregates with the β-sheet structure grow and transform into a mature fibril. These two stages of amyloid formation have been recently observed and investigated in computer modeling of the protein aggregation process (15) based on the tube model of protein (16), and the nucleation barriers for aggregation and fibril elongation have been characterized.

The stability and propensity for aggregation of Aβ peptides constituting Aβ fibril are significantly affected by the (familial) point mutations. The effects of mutations

Submitted May 30, 2008, and accepted for publication September 17, 2009.

*Correspondence: andriy.kovalenko@nrc-cnrc.gc.ca

Editor: Edward H. Egelman.

0006-3495/10/01/0282/15 $2.00

doi: 10.1016/j.bpj.2009.09.062

have been extensively studied for the different stages of oligomerization and fibril formation using various computational approaches. Initial misfolding and conformation dynamics of Aβ monomers were analyzed, based on all-atom explicit solvent molecular dynamics (MD), Monte Carlo methods, and coarse-grained models (17–23). It was found, for example, that the difference in the oligomerization propensity for different mutants can be related to the change in stability of Aβ peptides upon mutation (17,18,22,23). This finding is in agreement with the recent experimental studies on the familial mutations of Aβ peptides (24). Another set of the theoretical works have been focused on the properties of Aβ oligomers. Because their structure remains unknown, the dynamics and thermodynamic of Aβ aggregates have been analyzed for the β-sheet oligomers modeled after the fragment of mature fibril (21,25–31). Most of these studies relied on the recently proposed high-resolution molecular models of Aβ_{1-40} (6,7) and Aβ_{1-42} (8) fibrils. Such β-sheet oligomers can be possibly generated in vivo or in vitro by fragmentation of the mature fibril. It was recently found that Aβ dimer (with the still unknown molecular structure) is the smallest neurotoxic agent in the Alzheimer's disease, and such dimers may be released by the amyloid fibril (32). One may speculate that after dissociation from the fibril, small oligomers may initially preserve their cross-β structure, with further major structural reconstruction. The accuracy of this hypothesis has yet to be confirmed, but the analysis of dynamics and thermodynamic stability of β-sheet oligomers has been proven to provide an important insight into the pathways of oligomerization and to assist in modeling of the structure of Aβ oligomers (21,25–31).

In this article, we focus on the comparative study of the association thermodynamics and conformational stability of the β-sheet wild-type Aβ_{17-42} oligomers with the different charge state of solvent-exposed Glu^{22}, and the E22Q (Dutch) mutants. The E22Q mutation (33,34) substitutes the polar (negatively charged at neutral pH) glutamic acid with the polar (neutral) glutamine residue at position 22 in the Aβ peptide, which reduces its charge. The Dutch E22Q mutants are characterized by higher oligomerization propensity and fibril elongation rate, compared to the wild-type Aβ peptides (13,35–39), and the Dutch mutation may promote stability of Aβ_{1-40} aggregates (13). It was proposed that the reduction in the direct electrostatic interactions upon mutation can destabilize the turn (Val^{24}-Gly^{25}-Ser^{26}-Asn^{27}) in the Aβ monomers, which makes them less stable, and promote the aggregation (17,24). In addition, the decrease in the electrostatic penalty may be a favorable factor in the oligomerization process after the initial conformational change of the monomer (21–24). For the wild-type (WT) peptides, a similar alternation of the charge state at position 22 can be due to protonation of the glutamic acid residue upon lowering solvent pH. It was proposed in Massi et al. (22) that the fibril elongation rate for the WT and the Dutch mutant peptides may be similar under acid conditions. The analysis of pK_a of the protonatable residues shows that for pH 4 and below, solvent-exposed Glu^{22} residues will be protonated. The comparison of the thermodynamic properties of the E22Q mutants and the WT assemblies at pH 4 is of interest because of their similarity regarding the direct electrostatic interactions. We note that at pH 4 the oligomerization may proceed through a different route, compared to the neutral solvent environment, and the resulting morphology of the oligomers or fibrils may be different from that corresponding to the WT pH 7 or the Dutch mutant cases (40).

Solvation effects play a significant role at different stages of formation of prefibrillar oligomers and amyloid fibrils. Theoretical description of solvation effects requires statistical mechanical approaches to the solvation structure and thermodynamics. All-atom explicit solvent MD can be referred to as a first-principle approach to the structural and thermodynamic properties of biomolecular systems (41). MD methods have been used to study different aspects of amyloidogenesis, from unfolding of amyloidogenic proteins to oligomerization and fibril formation (17–23, 25–29,42–57). Study of the thermodynamics of oligomerization and formation of amyloid fibrils using the MD simulation approach has been significantly impeded by the enormous complexity of the problem. First of all, the thermodynamic analysis of large aggregates of proteins is a notoriously computationally demanding problem. Even modern powerful computers do not allow one to simulate, from the first principles, the effects of solvation on aggregation, fibrilization, and stability of oligomers and amyloid fibrils, with systematic accounting for solvent composition and its properties such as level of pH and salt concentration. Decomposition of the free energy (including the solvation part) into its physical components, such as entropic and enthalpic, electrostatic and nonelectrostatic, which provides essential information on mechanisms of proteins folding and aggregation, is currently also impractical in MD simulations (and indeed unfeasible for large protein aggregates in realistic systems), both with explicit and implicit solvation models. In the latter case, the nonelectrostatic interactions, and thus, hydrophobic effects which are crucial for correct explanation of the mechanisms of misfolding and aggregation of amyloidogenic proteins, cannot be accounted for in a proper way (58,59). Additionally, the MD description of solvent molecules buried inside the protein folds and possibly localized in the core of amyloid fibrils at the different stages of the maturation process requires modeling of nonequilibrium events of folding/unfolding and aggregation to allow the solvent molecules to penetrate the structure. This is a challenging problem for current MD simulations for large biomolecular systems.

The above explains why there has been no thorough study of solvation effects so far, despite the importance of solvation effects for the pathways of misfolding and aggregation of amyloidogenic peptides. Here, making the first step in this direction, we present a comprehensive analysis of the association thermodynamics, including the solvation effects

on the thermodynamic stability of small A$\beta_{17–42}$ oligomers with pronounced β-sheet structure, obtained by fragmentation of mature fibril. We achieve that by employing the statistical-mechanical, three-dimensional molecular theory of solvation (60), also known as 3D-RISM-KH approach. The method has proven to be successful in the description of the solvation structure and thermodynamics of proteins and protein complexes under different solvent conditions (61–70).

METHODS

Free energy calculations

The free energy of a macromolecule in solution can be represented as an average over all possible conformations sampled from the canonical distribution (71),

$$\Delta G = \langle \Delta H_{\text{gas}} \rangle + \langle \Delta G_{\text{solv}} \rangle - T\langle \Delta S_{\text{conf}} \rangle, \qquad (1)$$

where the first two terms give the effective energy of a macromolecule in solution (71,72), and the last term is the contribution to the free energy due to the macromolecule conformational entropy. The gas-phase internal energy includes the bonded (bond, angle, and torsion angles) and nonbonded (the van der Waals or dispersion, and the electrostatic) interactions. The solvation free energy, ΔG_{solv}, is the free energy change upon transfer of the solute molecule from vacuum to solvent. It describes all the solvation effects, including those due to the solvation energy and entropy. The angle brackets denote the average over conformations sampled from the canonical distribution for the solute-solvent system at given temperature T, using the MD or Monte Carlo methods. The above equation is a theoretical basis for the molecular mechanics-Poisson-Boltzmann/Surface Area (MM-PB/SA) approach for calculation of the free energy of macromolecules in solution (73–76), as implemented in the AMBER MD package (77). The approach was previously used to study the thermodynamics of amyloidogenic peptides in Ding et al. (78).

There is growing evidence that the continuous solvation models, such as the Poisson-Boltzmann approach combined with the solvent-accessible surface area (SA) term to account for the nonpolar interactions, cannot describe the nonelectrostatic effects accurately (58,59,74), especially for small proteins. This follows from the fact that for small peptides there is no proportionality between solvent-accessible surface area of a protein and the nonpolar part of the solvation free energy (79). In addition, such models do not account correctly for the dispersion interactions and excluded volume effects (58,59). This raises questions about their applicability to describe quantitatively the hydrophobic effects, which are of paramount importance for understanding the molecular mechanisms of misfolding and aggregation of amyloidogenic proteins (15). Here, to account accurately for nonpolar effects on the association thermodynamics of A$\beta_{17–42}$ peptides, we propose the following combined approach. We use molecular dynamics (MD) to generate trajectories, followed by molecular mechanics (MM) to calculate the peptides internal energy and conformational entropy and the three-dimensional molecular theory of solvation to characterize the solvation free energy. It worth noting that the continuous solvation models, such as the Poisson-Boltzmann or generalized Born methods combined with the solvent-accessible surface area nonpolar term, require the phenomenological parameters (ionic radii, the surface tension coefficients) to be used as input for modeling (74), which makes them less reliable, compared to the molecular theory of solvation.

Following the same lines as in the original implementation of the MM-PB/SA approach, we first performed all-atom explicit solvent MD simulations for A$\beta_{17–42}$ oligomers of different sizes. Then, the gas-phase energies and the conformation entropy of the oligomers were found using the *sander* and *nmode* modules of the AMBER 9 molecular dynamics package (77) (the MM part of the simulations). The solvation free energy and its components were obtained using the 3D-RISM-KH approach (60). The combination of the MM and the molecular theory of solvation will be referred to as the MM-3D-RISM-KH method. The approach is currently being implemented in the AMBER package (80) and will be available in its new releases.

Molecular dynamics simulations and energy minimization

MD trajectories for free energy calculations were obtained from the all-atom explicit solvent molecular dynamics simulations using the AMBER 9 molecular dynamics package (77) with the ff99 protein force field (81). As a starting conformation for modeling, the experimental structure of the fragment of Aβ fibril (Protein Data Bank ID code 2BEG (8), model 1) was used. The fragment consists of five Aβ (1–42) peptides (8) labeled A, B, C, D, and E. To avoid conformational bias we analyzed only the part of the fragment with the well-defined secondary structure that corresponds to residues from 17 to 42 for each Aβ peptide. Their coordinates were taken from the PDB file. The similar construct was recently used for modeling the Alzheimer fibril architecture (25). The initial structure for A$\beta_{17–42}$ pentamer comprised all five chains (from A through E) of the experimental structure. As a representative (starting) conformation for A$\beta_{17–42}$ monomer, chain C was used. The initial structures for other complexes were made of chains B and C in the case of a dimer, chains B, C, and D for a trimer, and from chains B, C, D, and E for a tetramer. The initial structures for the Dutch mutants were obtained by the E22Q substitution using the AMBER 9 molecular dynamics package (77). To simulate the solvent acidic condition at pH 4, we first found the change in the charge state of the A$\beta_{17–42}$ peptides upon lowering the pH. We used the PROPKA 2.0 software (82) to obtain pK_a values of the protonatable residues. Then, based on this information, we updated the charge states of these residues. The pK_a values of the solvent-exposed glutamic acids Glu^{22} fall into the range between 4.5 and 4.8, which allowed us to suggest that lowering the level of pH below 4.5 will result in protonation of these residues. Because pK_a values for all other solvent-exposed residues are >7 or <4, there will be no further changes of the protonation states of the peptides. Protonation of the solvent-exposed glutamic acids results in neutralization of each peptide. Thus, the interval of pH between 4 and 4.5 corresponds to the isoelectric point of the A$\beta_{17–42}$ peptides as it is predicted by the PROPKA algorithm (82). We note that the structure of the amyloid fibril and the pathways of oligomerization may be different at low pH conditions compared to both the wild-type at the neutral pH and the E22Q mutant cases, and the above models were used only as initial conformations for the molecular dynamics simulations.

In all MD simulations, the following protocol was used. In the WT pH 7 case, the sodium counterions were added with the AMBER package at the points of the lowest electrostatic potential to compensate nonzero charges of peptides ($-1e$ per monomer, where e is the elementary charge). The initial structures were solvated with SPC/E (83) water molecules in a rectangular periodic box. A distance of at least 20 Å was allowed between the peptides and periodic boundaries to avoid any bias due to the periodicity of the simulation box. The number of water molecules added varied from 9910 (in the case of the monomer) to 12,825 (for the pentamer). The above procedure was followed by two minimization runs. In the first run, to relax solvent, we used 5000 steps of the steepest descent method followed by 5000 steps of the conjugate gradient method, keeping peptides' degrees of freedom restrained. In the second run, an additional 5000 of the steepest descent cycles were used to relax the peptides' degrees of freedom. For the minimized systems, the root mean-square (RMS) of the energy gradient was <0.015 kcal/(mol Å).

The production MD simulations were preceded by two thermalization/equilibration runs. First, the temperature was gradually raised from 0 to 298.15 K and the system was thermalized for 50,000 MD steps. Then, another portion of 50,000 MD steps at constant pressure were used to relax the solvent degrees of freedom and to adjust the solvent density to ~1 g/cm^3. For pressure regulation, the isotropic position scaling was used with the pressure relaxation time of 1 ps^{-1}. In both equilibration runs the peptides coordinates were restrained to their minimum energy values. The MD

step was set to 1 fs. In the production runs, all bonds involving hydrogen atoms were constrained with the SHAKE algorithm (84), which allowed us to set the MD step to 2 fs. Langevin dynamics was used for temperature control with the collision frequency of 5 ps^{-1}. The cutoff for nonbonded interactions was 16 Å. The other parameters in *sander* were set to their default values.

For the free energy calculations, snapshots were taken every 20 ps from a 0.5-ns stretch of the metastable part of the MD trajectories for each complex. These snapshots were then used to find averages of the free energy components, according to Eq. 1. The number of snapshots taken for postproduction analysis was limited by the computational time of this approach. The most time-consuming parts are calculations of the conformational entropy of peptides using module *nmode* from the AMBER 9 molecular dynamics package (77) and of the solvation free energy (and its breakdown into energetic and entropic components) using the three-dimensional molecular theory of solvation. To verify the approach we also calculated the gas-phase energies of peptides using all 2500 snapshots taken from the same parts of the trajectories. The deviations from the partial average were <1–11 kcal/mol, depending on the oligomer size. This is less than the standard deviation for any component of the free energy. Additionally, calculations of the free energy were carried out, based on the sets of snapshots selected with different clustering algorithms implemented in *ptraj* module from the AMBER 10 molecular dynamics package. The averages obtained using different techniques agree within 3–7 kcal/mol, depending on the oligomer size. Thus, the number of representative snapshots used for analysis was large enough to control the standard error at the appropriate level.

Three-dimensional molecular theory of solvation

The molecular theory of solvation is based on the formally exact formulation of the statistical mechanics in terms of integral equations for density-density correlation functions for all components of a system (85). As required for any analytical theory, it requires some approximations before it can be used as a practical tool in biosimulations. The reference interaction site model (RISM) theory in its classical formulation (86,87) allows one to reduce dimensionality of the theory, reformulating it in terms of one-dimensional correlation functions. This approach has been used successfully to describe thermodynamic and structural properties of molecular and atomic liquids and mixtures of a given composition, including electrolyte solutions (87). Its three-dimensional extension (3D-RISM) (60,88,89) successfully predicts the solvation structure, thermodynamics, and volumetrics of numerous macromolecules, especially for those of proteins in solution (60–70). A key component of the theory is a closure relation complementing the integral equation for the solute-solvent site total and direct distribution functions. In our study, we employ the approximation proposed by Kovalenko and Hirata (3D-KH closure) (60,89), which has been proven to be appropriate for complex systems with strong charges and associating bonds, including proteins in aqueous solutions (60–70,90). The accuracy of the approach is comparable with all-atoms explicit solvent simulations of the solvation free energy. In contrast to the implicit solvation models, such as the Poisson-Boltzmann or its approximation by the generalized Born model (often combined with the solvent accessible surface term to account for the nonelectrostatic interactions), the 3D-RISM approach treats both the electrostatic and nonelectrostatic interactions on the same footing, much as all-atoms molecular simulations with explicit solvent do. It worth mentioning that the nonelectrostatic interactions are related to the hydrophobic effects, and thus their accurate description is crucial for understanding of the molecular mechanisms of fibrilization. An attractive feature of the theory is that it analytically yields the solvation thermodynamics and volumetrics, including the solvation entropy (60). What makes this method unique in biomolecular simulations is the possibility to correctly account, from the statistical mechanical principles, for solvent molecules trapped inside biomolecular complexes (62). Such localized pockets of solvent are of paramount importance for stability of aggregates of proteins, but in many cases cannot be adequately described in explicit solvent molecular dynamics simulations, because allowing the solvent molecules into the protein cavity requires simulating a complete refolding event.

The method we use in this study and its application for proteins have been reviewed elsewhere (60,65), and we provide a brief description of the approach in the Supporting Material. The theory yields complete information on the solvation thermodynamics, including the solvation free energy, ΔG_{solv}, and solvent distributions around proteins. To get insight into thermodynamic stability of small Aβ oligomers, we decompose the solvation free energy into the energetic and entropic components (65,91), $\Delta G_{solv} = \Delta E_{solv} - T\Delta S_{solv}$. The hydration entropy ΔS_{solv} (in NVT ensemble) is calculated as the temperature derivative of the solvation free energy at constant solvent density, $\Delta S_{solv} = -(\partial \Delta G_{solv}/\partial T)_{\rho}$.

RESULTS AND DISCUSSION

Conformational stability of $A\beta_{17–42}$ oligomers

Even for small peptides, many different folding (unfolding) pathways exist which may span over a microsecond timescale (92). For $A\beta_{21–30}$ monomers, for example, it was found in all-atom explicit solvent simulations that the major conformational changes occur on the timescale of hundreds of nanoseconds (18). The process of dissociation of small β-sheet oligomers are characterized by similar timescales, as observed in the MD study of the stability of Aβ oligomers with β-sheet structure (28,29). Thus, for the small $A\beta_{17–42}$ complexes studied in this article, the dissociation (association) and refolding times may exceed the microsecond scale. Full conformational sampling for such systems with available computational resources is currently unfeasible. At the same time, the dynamics on the shorter time intervals may be characterized by dynamically metastable states associated with different basins of the energy landscape, and thus it provides useful insight into particular stages of oligomerization. In addition, the balance between components of the free energy derived from the relatively short (compared to the timescale of folding/association event) MD simulations gives important quantitative information about the driving forces behind the association of Aβ peptides and the molecular mechanisms of the thermodynamic/dynamic stability of oligomers. The main goal of our study is to elucidate these mechanisms for small β-sheet oligomers obtained by fragmentation of the mature Aβ fibril, with special emphasis on the solvation effects—in particular, for those of solvation entropy.

The conformational changes of the oligomers in the course of the MD simulations were monitored by the root mean-square displacements (RMSDs) and mean-square fluctuations (MSFs) of the backbone atoms (Figs. 1 and 2). The RMSDs provide useful information on relative stability of the oligomers, and were previously used in stability analyses of Aβ oligomers with β-sheet structure (25,27,28,42). Because the starting conformations were modeled after the fragment of the mature fibril and which, thus, are not true (experimental) structures of small Aβ oligomers, the reconstruction of the complexes took place at the beginning of the production MD runs. In agreement with the previous

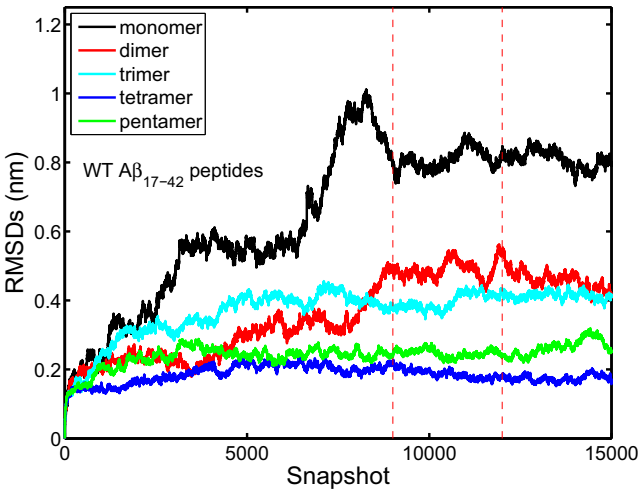

FIGURE 1 Root mean-square displacements of the backbone atoms from the initial structures in the production MD simulations for the wild-type Aβ_{17-42} monomer, dimer, trimer, tetramer, and pentamer with the charge state corresponding to neutral pH. (*Vertical lines*) Dynamically metastable parts of the trajectories used for the free energy calculations. Conformational changes monitored by the RMSDs demonstrate a similar dependence on the system size for the WT pH 4 and the E22Q mutants.

studies, we found that the extent of the conformational changes strongly depends on the complex size. The most dramatic changes occur for the monomers, followed by those for the dimers and trimers. For the larger constructs, less significant distortion of the initial β-structure was observed on the timescale of the simulations. After ~2 ns of MD runs, the RMSDs for the monomers and dimers reach plateaus that can be regarded as the signature of a dynamically metastable state. The conformational fluctuations (as seen from RMSDs and MSFs) are still significant, but they take place around some reference (average) structures, which show the conformational changes on much longer timescales. The Aβ_{17-42} dimers are characterized by less flexibility, compared to the monomers, as clearly seen from the evolution of the RMSDs and MSFs, and from the inspection of the MD snapshots. Contrary to the monomer case, some reminiscence of the β-strand geometry and the β-sheet structure of the mature fibril are partly preserved in the dimers on the nanosecond timescale, mostly at the N-terminal parts of the peptides (the origin of this asymmetry between the N- and C-termini will be discussed below). For the Aβ_{17-42} trimers, tetramers, and pentamers, the plateaus attributed to the dynamically metastable state are reached earlier in the course of MD simulations, compared to the monomer and the dimer cases. The conformations corresponding to the metastable states for the tetramer and pentamer are characterized by the significantly smaller RMSDs.

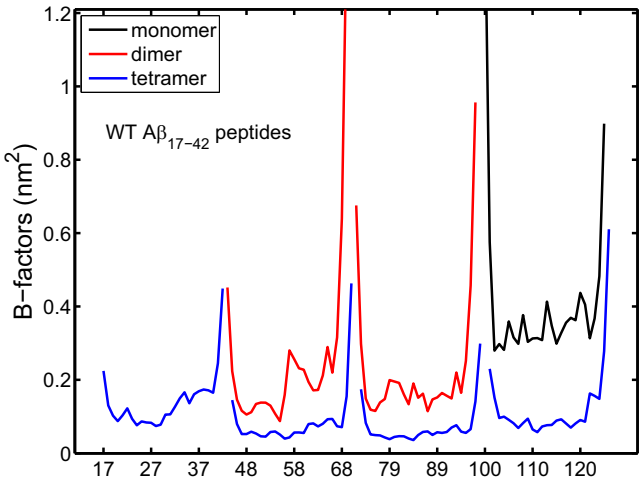

FIGURE 2 Mean-square fluctuations (B-factors) of the α-carbon atoms on a per-residue basis for the wild-type Aβ_{17-42} monomer, dimer, and tetramer at neutral pH. B-factors are normalized as follows: $B_i = 8\pi^2/3\langle \Delta \mathbf{r}^2_i \rangle$, where the angle brackets denote an average over MD conformations.

Whereas the RMSDs show structural deviations of the oligomers from the initial conformations in the course of MD simulations, the MSFs provide insight into flexibility of the oligomers. In Fig. 2 we present the MSFs of the α-carbon atoms normalized to give the dynamic B-factors which are used for interpretation of x-ray scattering experiments. The analysis of the B-factors reveals few common dynamic characteristics for all constructs and all oligomer sizes. As it was anticipated (25–27,42), the N- and C-termini are the most flexible parts of the peptides for all the systems. The enhanced flexibility is also observed in the turn region (Ser^{26}-Ile^{31}) and at the glycine residues. The inter- and intrapeptide salt bridges between Asp^{23} and Lys^{28} residues reduce the local flexibility. For most oligomers, the N-terminal part of the Aβ_{17-42} peptides demonstrates the reduced flexibility compared to the C-terminus. As we will show below, this can be attributed to the stabilizing role of the salt bridges and also partly to the hydrophobic attractions between residues from the central hydrophobic cluster located at the N-terminus of the Aβ_{17-42} peptides (residues 17–21). The increase in flexibility at the C-terminus can be explained in part by the disruption of the network of hydrogen bonds and resulting loss of the β-sheet secondary structure. In the N-terminal parts of the oligomers, the secondary structure is preserved because of the two favorable factors discussed above: 1), the inter- and intrapeptide salt bridges; and 2), the hydrophobic interactions between the residues from the central hydrophobic cluster. For the monomers, however, the N-terminus is characterized by the enhanced flexibility—which may indicate the tendency to bury the hydrophobic residues in the interior of the peptide fold.

There is an overall trend in the flexibility to increase from the N- to C-terminus and from the left chains (solvent-exposed Lys^{28} and the central hydrophobic cluster) to the right chains (solvent-exposed Asp^{23}) for the all models of the Aβ_{17-42} oligomers. At the same time, the far left chains of the larger complexes (starting from the trimer) demonstrate enhanced flexibility similar to that of the far right

chains. This observation suggests that the dissociation (and, possibly, association) at the different edges of β-sheet Aβ aggregates and mature fibrils may follow different routes. The asymmetry in the flexibility reflects the fact that the salt bridges between Asp^{23} and Lys^{28} have more stabilizing effect on the N-terminal part of the peptides in the β-sheet oligomers, and is also the consequence of the more pronounced hydrophobic interactions in the N-terminal domains of the peptides. The discussed asymmetry in the physical interactions (and resulting increase in the flexibility) may be responsible for the observed structural twist of the oligomers and the chirality of the protofilaments.

Association thermodynamics of Aβ_{17-42} oligomers: effects of the E22Q mutation and protonation of Glu^{22}

We assess thermodynamic stability of the Aβ_{17-42} oligomers of different size in terms of the association free energy. Averaging the instantaneous values of the components of the solvation free energy, the gas-phase internal energy, and the conformational entropy of the peptides over the representative snapshots taken from the MD trajectories as discussed in Methods, we obtain the estimates for the free energy of the WT and the Dutch mutant Aβ_{17-42} oligomers and monomers. Then, we find the association free energy for each model as a difference between the free energy of an oligomer and that of constituting monomers. The association free energy and its components for the WT oligomers at pH 7 and 4, and for the E22Q mutants, are plotted in Figs. 3–5 as a function of the oligomer size. As seen from Fig. 3, the association free energy of these small β-sheet oligomers shows near-linear trend with the dimers being thermodynamically more stable compared to the larger complexes. The latter is in agreement with the experimental data (93). The linear (within statistical uncertainty) dependence of the association free energy on the complex size is a consequence of the unilateral stacking of monomers in β-sheet oligomers. Whereas for the neutral peptides (the WT pH 4 constructs and the Dutch mutants) such size evolution of the association free energy is an expected result, it is less obvious why the same is true for the charged peptides with the significant contribution of the long-rang electrostatic interactions to the association thermodynamics. We will show below that this can be explained by the complementarity between the gas-phase and solvation electrostatic effects. It is worth mentioning that the linearity in the association free energy is related to the β-sheet structure of the oligomers (formation of the interstrand β-sheets is responsible for the unilateral stacking), and possible structural reconstruction of the oligomers and/or the reduction of their β-sheet content may result in the deviation from such behavior.

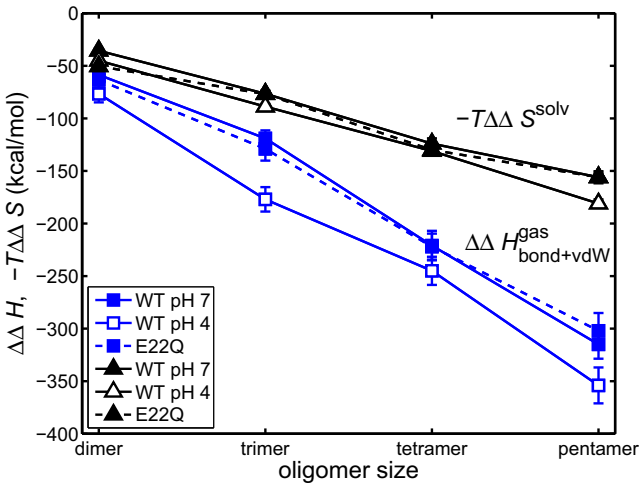

FIGURE 4 Solvent entropic and interpeptide nonpolar contributions to the association free energy for the wild-type Aβ_{17-42} oligomers and the E22Q mutants.

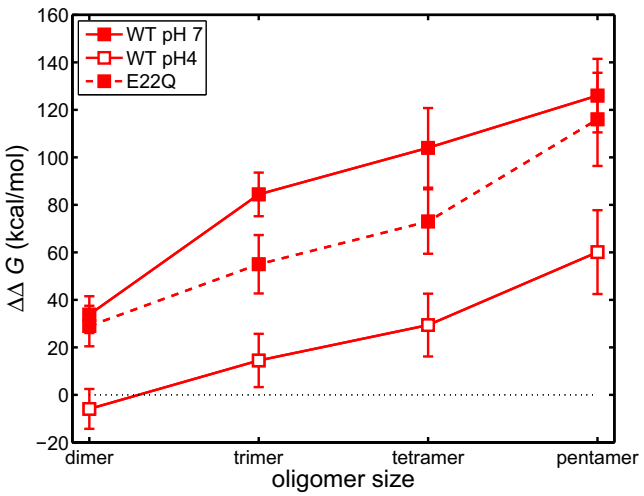

FIGURE 3 Association free energy of the wild-type Aβ_{17-42} oligomers and the E22Q mutants as a function of their size.

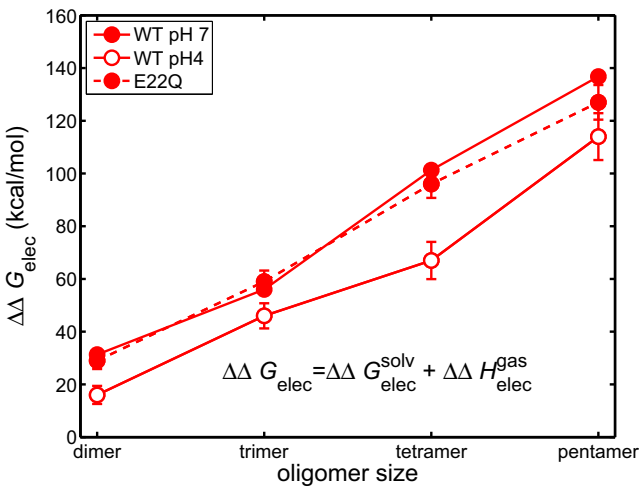

FIGURE 5 Size evolution of the electrostatic part of the association free energy for the wild-type Aβ_{17-42} oligomers and the E22Q mutants.

The oligomers partially preserve their β-sheet structure in the MD runs over the nanosecond timescale. Whereas the structures of the monomers and the dimers significantly depart from the initial conformations (as it follows from the RMSDs shown in Fig. 1), the larger complexes are relatively stable and keep their β-sheet structure over long time. At the same time, the association free energy is positive for most oligomers (the WT pH 4 Aβ_{17-42} dimer with the neutral charge may be an exception). This suggests that there are two possibilities:

1. Further reconstruction of the oligomers may take place over longer timescales, resulting in lowering of the association free energy; and
2. Thermodynamically stable states do not exist for small Aβ_{17-42} oligomers.

The latter agrees with the nucleation-polymerization mechanism of the fibril formation and the existence of the critical size of the fibrilization nucleus (1,12,13). It is worth mentioning that the association effective energy, defined as a sum of the solvation part of the association free energy (including the solvation entropic component) and the association gas-phase internal energy (71,72), remains negative for most oligomers sizes (see Fig. S2 in the Supporting Material). Moreover, the association effective energy decreases with the complex size. This means that the conformational entropy (not included in the definition of the effective energy (71,72)) is one of the major destabilizing factors in the association thermodynamics of the β-sheet oligomers, and the conformational changes in the oligomers leading toward their stabilization may result in the reduction of the conformational entropic penalty.

Our calculations demonstrate a much lower association free energy for the β-sheet WT oligomers at pH 4, compared to the WT pH 7 and the E22Q mutant cases. In addition, the neutralization of the peptides in acidic environments may result in stabilization of the Aβ_{17-42} dimers. This indicates that the pathways of the fibrilization can be different in the lower pH solvent environment compared to both the neutral pH and the E22Q mutant cases. In particular, the fibrilization through the oligomerization pathway may be a thermodynamically favorable process, in agreement with the experimental data (40). It was shown experimentally that the E22Q mutant demonstrates a higher oligomerization propensity compared to the WT pH 7 case (35–39). In our calculations, we found no statistically significant difference between the association free energy for the Dutch mutant and the WT pH 7 β-sheet oligomers (see Fig. S1 for the details of the convergence study). It may mean that the difference in the oligomerization propensity is defined by the early stages of aggregation, namely, the conversion of Aβ monomers from the random coil to the β-sheet conformation. The latter is in agreement with the previous experimental and theoretical studies of the effects of the Dutch mutation on the pathways of association of Aβ peptides, which attributed the higher oligomerization propensity of the mutants to a conformational transition in the Aβ monomers before the oligomerization or in the process of the monomer deposition (17–24,31,35,37).

The E22Q oligomers have a charge distribution (on a per-residue basis) similar to that of the WT pH 4 oligomers. Thus, the difference in the association free energy between the WT peptides and the E22Q mutants cannot be explained only by the difference in the electrostatic interactions. Obviously, the reduction of the peptide charge due to mutations or protonation of the solvent-exposed protonatable residues at acidic conditions reduces the direct electrostatic interaction between peptides. Additionally, the solvation structure around the peptides depends on the charge distribution which may affect both the solvation entropy (hydrophobic interactions) and the solvation energy. To understand the exact balance between the different physical components of the association free energy, we decompose the association free energy into the nonpolar gas-phase (internal) part, the solvation entropic contribution and the electrostatic part. The electrostatic part accounts for the direct inter-/intrapeptides electrostatic interactions and also includes the electrostatic component of the solvation free energy. We compare the above physical components of the association free energy for the WT pH 7, pH 4, and the Dutch mutant assemblies as a function of their size in Figs. 4 and 5. For the neutral WT peptides, the electrostatic effects, the solvation entropic effects, and the nonpolar interactions (the gas-phase bonded and the van der Waals interactions) all are important factors that contribute to the lowering of the association free energy with respect to the WT pH 7 and the E22Q cases. For the Dutch mutants, the reduction in the direct electrostatic interactions due to the E22Q substitution is mostly compensated by the unfavorable change in the electrostatic part of the solvation free energy (these components of the association free energy are represented in Fig. S3). The difference in the overall electrostatic contribution to the association free energy between the charged WT pH 7 peptides and the neutral E22Q mutants is within the statistical error range. In the case of the charge neutralization due to protonation of Glu^{22} residue at acidic conditions, the above compensation is not complete—which results in the lowering of the electrostatic contribution to the association free energy for the WT pH 4 oligomers with respect to the WT pH 7 and the Dutch mutant cases. We also note that the charge neutralization at position 22 due to protonation of Glu^{22} or the E22Q mutation may alter the formation of salt bridges between Asp^{23} and Lys^{28}. This affects the contributions of the direct (intra- and interpeptide) electrostatic interactions between these charged residues to the association free energy (see the discussion below). At the same time, the reduction of the overall electrostatic penalty due to the neutralization/substitution of Glu^{22} is not that significant, as it might be expected, because it is mostly compensated by the increase in the solvation energy. The compensation is possible because the side chain of Glu^{22} is solvent-exposed and fully

solvated in the β-sheet oligomers, much as in the proposed models of the amyloid fibril (6–8).

The difference in the gas-phase nonpolar interactions between the neutral WT oligomers at pH 4 and the other constructs can be explained by the larger extent of reconstruction of the initial structure of the oligomers in the former case. This is a result of the destabilization of the salt bridges between Asp^{23} and Lys^{28}, which leads to more favorable packing of the peptides in the oligomers. The favorable reduction in the solvation entropic part of the association free energy (directly related to the hydrophobic interactions) upon the neutralization of the peptides is a more subtle effect. It can be observed for both the neutral WT and (to a lesser degree) the E22Q mutant. As we show below, the effect can be traced-down to the modification of the microscopic solvation structure around the peptides as a result of their neutralization.

In addition to the obvious differences in the association thermodynamics for different $A\beta_{17–42}$ complexes, there are common basic principles behind the thermodynamic properties for all β-sheet oligomers, regardless of their charge state or sequence. The solvation entropic effects and the interpeptide van der Waals interactions are the two most favorable factors contributing to stability of oligomers. The solvation entropic effects are directly related to the hydrophobic interactions, and therefore the above results (see Fig. 4) highlight a key role of hydrophobicity in the formation and stability of the Aβ assemblies. Fig. 4 also provides the quantitative characteristics of the hydrophobic effects for the WT and Dutch mutant $A\beta_{17–42}$ oligomers as a function of their size. In part, hydrophobicity is related to the disruption of the network of hydrogen bonds between water molecules and formation of the hydrogen bonds between water and solute molecules—a phenomenon fully accounted for in the framework of the molecular theory of solvation (87). Although the hydrophobic interactions is a significant factor driving the process of oligomer assembly and formation of the mature fibril, it should be considered together with the unfavorable solvation energetic effects in the context of thermodynamic stability of the oligomers and fibrils under different solvent conditions. In the gas phase (and also in nonpolar solvents or in polar solvents at reduced density), there are no favorable hydrophobic interactions and, at the same time, no solvation energetic penalty is present. In such situations, the energetic balance is shifted toward the gas-phase energy and the conformation entropy of the peptides. This can partly explain the observation of the α-helical conformation in the MD simulations at the reduced solvent density (18), and also the difference in the physical properties between wet and dehydrated fibrils.

In contrast to the favorable solvation entropic effects, the change in the conformational entropy inhibits the association of the peptides. This is due to the obvious reduction of flexibility of a peptide upon its association with the Aβ complex. Interestingly, there is a complementarity (partial compensation) between the solvation and conformational entropic contributions for all oligomers. As a consequence, the size evolution of the association free energy and enthalpy are similar. Because the physical mechanisms behind the solvation entropic and the conformational entropic effects are quite different, it is a rather interesting observation.

The overall effect of the screened Coulomb interactions (the gas-phase electrostatic interactions combined with the electrostatic part of the solvation free energy) is to inhibit the process of aggregation and destabilize the oligomers. This does not exclude the favorable role of the specific electrostatic interactions, such as hydrogen bonds and salt bridges, which direct the formation of the oligomers and stabilize particular elements of the secondary structure (see the discussion of the local contributions to the free energy and the association free energy in the next section). Importantly, the balance between the different parts of the electrostatic energy, i.e., the gas-phase and the solvation parts, can be shifted by modification of the solvent properties such as the level of pH or ionic strength and also by the mutations that affect the overall charge of the peptides.

Because of the relatively short range of the van der Waals interactions (with respect to the electrostatic interactions) and their significant contribution to the association free energy (Fig. 4), one can conclude that the interpeptide interface in Aβ oligomers with a pronounced β-sheet structure (and also in Aβ amyloid fibrils) is characterized by a high degree of shape complementarity. This is in agreement with the previous modeling of shorter Aβ peptides (25). Such unusually tight shape complementarity is a signature of the dry interface of the steric zippers (5,4). It can be found in systems characterized by the cross β-structural motif, which is a characteristic of the Aβ fibrils (6–8). The dispersion interactions cannot be a driving force behind aggregation at the early stages of oligomerization, when the structure of amyloidogenic oligomers may be quite different from that of the mature fibril (1). At these early stages, the long-range electrostatic interactions and the hydrophobic effects are dominant. The specific electrostatic (including hydrogen bonding and formation of salt bridges) and hydrophobic interactions then direct further conformational transformation toward the higher complementarity of the interpeptide interface. At the last stages of oligomerization, the short-range van der Waals interactions lock the β-strands in the cross-β structures (44). This completes the formation of a seed required for the elongation step of the fibril growth (1,12,13).

Our calculations show that the small $A\beta_{17–42}$ oligomers with the pronounced β-sheet structure have positive association free energy, and thus they cannot be thermodynamically stable. Major structural changes may occur in the oligomers on the microsecond timescale and beyond, and they may lose structural similarity with the mature amyloid fibril or dissociate, as observed in some experiments (94–96). The structure of small Aβ oligomers studied experimentally may be

different from what one observes in relatively short MD simulations, and the resulting balance between different components of the association free energy may be shifted, compared to that discussed in our study. In particular, stability of oligomers with reduced β-sheet content can be enhanced by a smaller conformational entropy penalty upon their association.

Local contributions to the free energy and the association free energy

The association thermodynamics and conformational stability of the Aβ_{17-42} oligomers can be rationalized in terms of the local contributions of the major physical interactions to the free energy. Such an approach was previously used to study the free energy of the β-sheet dissociation in prion proteins (97). In this section, we mainly focus on the local direct (gas-phase) and solvation electrostatic effects to elucidate the favorable role of the specific interactions in the situation with the overall electrostatic penalty. The local nonpolar effects are also briefly discussed. We resolve the physical components of the free energy and the association free energy on a per-residue basis. To improve statistics, we average the data over all interior chains of the oligomers larger than trimers. The saltbridge-forming Asp^{23} and Lys^{28} residues are exposed to solvent in the monomers and dimers, and thus these systems should be treated separately. The local electrostatic contributions to the free energy and the association free energy of the β-sheet oligomers represented in Figs. 6 and 7, respectively, show the high level of specificity related to the formation of the network of interpeptide hydrogen bonds and the inter- and intrapeptide salt bridges between Asp^{23} and Lys^{28}.

In the N-terminal parts of the Aβ_{17-42} peptides, the dominant electrostatic contribution to the free energy is due to the charged (in the WT pH 7 case) Glu^{22}, Asp^{23} (negative charge), and Lys^{28} (positive charge) residues (Fig. 6). In the C-terminal domains, the oscillations of the electrostatic energy associated with the formation of the hydrogen bonds between the adjacent β-strands are clearly seen. The gas-phase part of the electrostatic energy (Fig. 6, *top panel*; note that the solvation effects are not included) shows, on the one hand, a qualitative difference in the interactions at position 22 between the WT pH 7 peptides, and on the other hand, the WT pH 4 and E22Q mutant peptides. This is an obvious consequence of the difference in the charge state at this location. Because of the complementarity between the direct (the gas-phase) electrostatic interactions and the electrostatic part of the solvation free energy, it is instructive to analyze their contributions together. We combine the gas-phase and the electrostatic part of the solvation energy obtained based on the generalized Born (GB) approximation, and show the result in Fig. 6 (*bottom panel*). The solvation electrostatic effects have a profound impact on the energetics of the solvent exposed residues. In particular, a major modification of the electrostatic energy due to solvation can be seen in the N- and C-termini for the all models, and at the location of solvent-exposed Glu^{22} for the WT pH 7 oligomers. A comparison of the electrostatic contributions for the different models of the Aβ_{17-42} oligomers shows that the electrostatic interactions at positions 22 (the proximity of the saltbridge-forming Asp^{23} residues) have the most stabilizing effect for the Dutch mutants, followed by the WT pH 7 and the WT pH 4 cases (Fig. 6, *bottom panel*). Although there are no direct correlations between the association thermodynamics data and the contributions of the specific electrostatic interactions, the latter in turn significantly affects the conformational dynamics of the oligomers because of destabilization of the inter- and intrapeptides salt bridges in the WT pH 4 case.

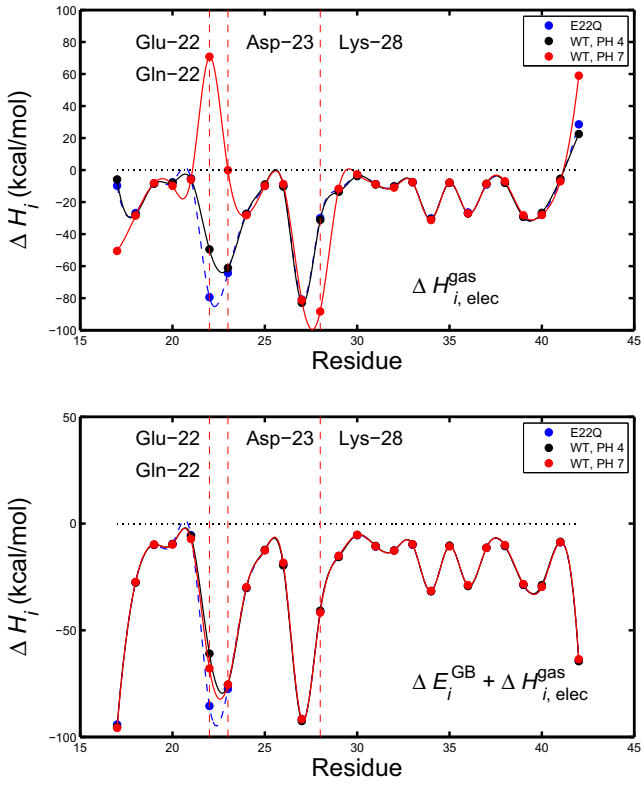

FIGURE 6 Local electrostatic contribution to the free energy resolved on a per-residue basis for the wild-type Aβ_{17-42} oligomers with the charge distributions corresponding to the solvent pH 7 (charged Glu^{22}) and pH 4 (protonated Glu^{22}) conditions, and for the E22Q mutant. (*Top panel*) Gas-phase electrostatic contribution. (*Bottom panel*) Gas-phase electrostatic energy combined with the solvation electrostatic energy. (*Vertical lines*) Location of Glu^{22} (the WT peptides) or Gln^{22} (the E22Q mutants), as well as the saltbridge-forming Asp^{23} and Lys^{28}.

The local electrostatic contributions to the free energy, from residues located at the different chains, strongly depend on the degree of their exposure to the solvent. For the β-sheet oligomers, the major differences may be between the peptide chains located at the edges of oligomers (amyloid fibril) and in the interior domains. In the fragment of the mature fibril used to model the initial conformations for our study, the Asp^{23} and

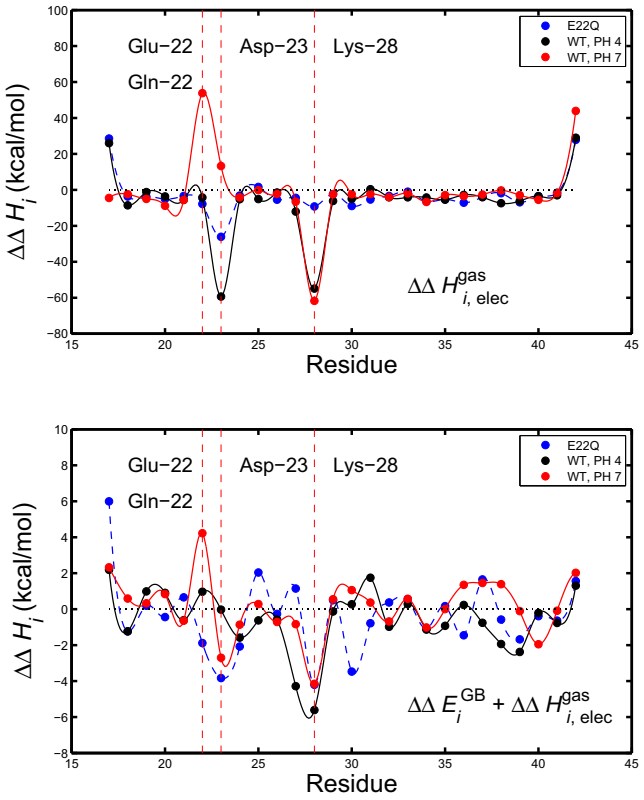

FIGURE 7 Same as in Fig. 6, but for the electrostatic contribution to the association free energy.

Lys^{28} residues form the interpeptide salt bridges (8). At the edges of the oligomers, these charged residues are partly exposed to solvent. This introduces the asymmetry (additionally to the asymmetry in the hydrophobic interactions (8)) between the edges of the β-sheet oligomers. For small oligomers, the desolvation of the charged residues due to the disruption of the interpeptide salt bridges and the formation of the intrapeptide ones may be an energetically favorable process resulting in destabilization of the β-sheet structure of the oligomers and eventually in their dissociation.

The local contributions of the different physical interactions to the association free energy on a per-residue basis can be obtained by calculating the difference between the local energies of the oligomers and the constituting monomers. The specificity of the nonbonded interactions is mostly due to the electrostatic interactions, and we show their local contribution to the association free energy in the top (the gas-phase part) and the bottom (the gas-phase part combined with the electrostatic solvation contribution) panels of Fig. 7. Clearly, the charged Glu^{22} residue introduces the local penalty toward association in the case of the WT pH 7 oligomers, and the solvation effects do not fully compensate this unfavorable effect as it had done for the free energy. It follows from the above comparison between the gas-phase and the overall electrostatic contributions that the electrostatic penalty is a consequence of the partial desolvation of Glu^{22} in the monomers upon their transfer from solvent to the oligomer, rather than a result of a direct repulsion between these charged residues. We also note that the electrostatic penalty at position 22 is present for the WT pH 4 oligomers with the protonated Glu^{22} residues, but in the much smaller scale, compared to the WT pH 7 case. No such penalty is observed for the Dutch mutants, which are characterized by the favorable electrostatic interactions both at the position of the mutation (Gln^{22}) and at the locations of the saltbridge-forming residues.

It is worth noting that the pattern in the local electrostatic interactions, on a per-residue basis for the free energy, is robust and may be characteristic of any Aβ oligomers. At the same time, the association free energy so-resolved relies on the conformational dynamics of the monomers. Because the major conformational changes for the monomers are expected beyond the nanosecond timescale, the local pattern in the association energy discussed in this study is characteristic of the stage of the conformational dynamics of the Aβ complexes currently accessible by MD simulations. The dispersion interactions resolved on a per-residue basis show a weak trend (with the exception of the monomers case where the interpeptide dispersion interactions are not present) of the increase from the N- to C-terminus. It indicates a more optimized packing of the side chains in the N-terminal part of the peptides. The favorable electrostatic and hydrophobic interactions between the residues in the central hydrophobic cluster are responsible for this effect. However, the tendency to optimize the nonbonded interactions in the N-terminal part of the peptides introduces the internal strains in these domains, which may overcompensate for the trend in the dispersion interactions.

Effect of charge substitution on microscopic solvation of Aβ_{17-42} oligomers

Neutralization of charged residues upon their protonation at low acidic conditions or as a result of point mutation has a significant impact on different components of the association free energy. The effect can be direct as in the case of the gas-phase Coulomb interactions, or can be related to the change in the solvation structure around oligomers. In the previous section, we have accounted for the solvent polarization effects in the framework of the generalized Born model, as shown in the discussion of the local contributions to the free energy and the association free energy (Figs. 6 and 7). Such a level of theory cannot describe the nonpolar solvation effects, and more importantly, the solvent reorganization and related solvation entropic effects contributing to the hydrophobicity. We have seen above that the solvation entropy is an important factor of stability of the Aβ_{17-42} oligomers. Here, we show how the Dutch mutation and protonation of Glu^{22} affect the microscopic solvation structure around peptides, and discuss the implications for the association thermodynamics.

The complexity of the solvation shells around the WT pH 7 Aβ_{17-42} pentamer is clearly seen from the left panel of Fig. 8. We show there the three-dimensional solvation maps for water oxygen (*red color*) and hydrogen (*blue color*) represented by density isosurfaces exceeding the bulk water density by a factor of 3. The density distributions for the solvent oxygen and hydrogen sites were obtained by using the 3D-RISM-KH approach. Additionally to the conventional information given by the solvent-accessible area, the three-dimensional molecular theory of solvation provides an insight into the balance between the oxygen and hydrogen distributions, and thus, into solvent polarization in the proximity of peptides. The observed microscopic structure of the solvation shells is a result of interplay between solute-solvent and solvent-solvent interactions (including, on the one hand, the hydrogen bonds between water molecules, and, on the other hand, hydrogen bonds between water molecules and solute). Local complementary in the oxygen and hydrogen distributions contributes to the lowering of the solvation free energy by reducing the electrostatic penalty due to the solvent-solvent interactions and also because of the reformation of the network of hydrogen bonds between water molecules in the proximity of the fibril. The water density around (inside) protein fold/aggregates can easily reach a value a few times larger than the bulk solvent density. The water molecules locked in the high density pockets can be regarded as structural water. The localized water molecules can be found in many locations around the oligomers and in the interior domains (see, for example, (25,26)). Their effect on stability of the assembly of Aβ peptides will be addressed in our subsequent study. Here, we note that the peculiarities in the solvation structure around the WT pH 7 Aβ oligomers indicate a possibility of formation of water bridges around the glutamic acid residues, and the water and ion channels inside the β-sheet oligomer core.

To demonstrate the effect of charge substitution on the microscopic solvation structure of the oligomers, we show the difference between the solvent densities corresponding to the oxygen site of water molecule for the WT pH 7 and the Dutch mutant pentamers in the right panel of Fig. 8. The most dramatic changes in the solvation structure occur at the locations of the point mutation (highlighted by the *red ellipse*), and in the domains of the enhanced flexibility (the loop domain and N- and C- termini). There is an obvious depletion of the solvent density in the proximity of Glu^{22}/Gln^{22} residues upon the charge neutralization. This indicates that for the Dutch mutants and also in the case of the oligomers with the protonated at low pH conditions solvent-exposed glutamic acids, the possibility of formation of the water bridges is ruled out. If such bridges formed at neutral pH, the above may contribute to the increase in the solvation free energy for these models, and may reduce their local conformation stability. It is worth mentioning that modeling the pH effects on thermodynamics of aggregation by accounting the static change in the protonation states of peptides is only an approximation that does not account for the dynamic aspects of the equilibrium between hydrogen ions in water and those at the protonatable residues exposed to the solvent. The implication is that the water bridges formed at neutral pH can delay the protonation of the solvent-exposed residues upon lowering pH, thus affecting the pathways of fibril formation and stability. In addition, the presence of water bridges at normal pH may increase the stability of the fibril formed at pH 7 relative to lower levels of pH, as it was found in experiment (98).

Another important aspect of the microscopic solvation of the Aβ_{17-42} oligomers, also related to the reconstruction of the structure of the solvation shells around peptides, is a more favorable solvation entropic contribution to the free energy for the Dutch mutant and the WT pH 4 oligomers, compared to the WT pH 7 case. The effect can be traced down to the differences in the local contributions of the solvation entropy, $-T\Delta S_{\mathrm{solv}}(\mathbf{r})$, to the solvation free energy

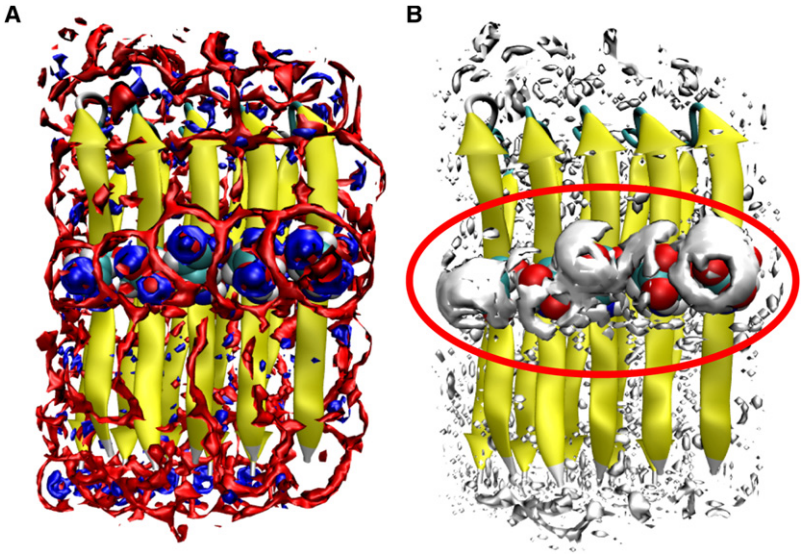

FIGURE 8 Effect of the Dutch mutation on the microscopic solvation structure around the Aβ_{17-42} pentamer. (*A*) Three-dimensional solvation density map for the wild-type pentamer represented by the isosurfaces of the distribution functions for water oxygen (*red color*) and hydrogen (*blue color*). Isosurfaces correspond to the water density exceeding the bulk density value by a factor of 3. (*B*) Change in the solvation structure upon the Dutch (E22Q) point mutation shown by the isosurface of the differential solvation density for water oxygen. Differential density is defined as the density excess for the wild-type oligomer with respect to that of the mutant. Isosurface value is 0.3. (*Red ellipse*) Location of the charged Glu residues substituted by the neutral Gln upon the Dutch mutation. Data shown is for the starting conformation used in MD simulations. Image was produced with VMD (99).

for the different oligomer models. We compare these contributions for the wild-type A$\beta_{17–42}$ to the Dutch mutant pentamer in Fig. 9. The more pronounced structure of the solvation shells for the wild-type oligomers are in agreement with the larger entropic contribution to the solvation free energy clearly seen in the left panel of Fig. 9. Compared to the Dutch mutant (Fig. 9, *right panel*), the major differences come from the proximity of charged Glu^{22} and from the interior of the oligomer (highlighted with the *red ellipse*). It is worth noting that the latter is not necessarily related to the internal solvation of the Aβ aggregates and amyloid fibrils discussed in the previous studies (25–27). The solvation entropy for the neutral (WT pH 4 and the Dutch mutant) oligomers are systematically lower compared with the WT pH 7 case for every snapshot of MD trajectory used in the calculations of the free energy. The reduction of the solvation entropic contribution upon peptides neutralization has implication for the association thermodynamics. As seen from Fig. 4, the solvation entropic contribution to the association free energy is lower for the WT pH 4 oligomers (and, to a lesser extent, for the Dutch mutants), relative to the wild-type oligomers with the charge distribution corresponding to neutral pH.

CONCLUSIONS

Using all-atom molecular dynamics simulation and the statistical-mechanical, three-dimensional molecular theory of solvation (also known as 3D-RISM-KH) combined with molecular mechanics, we have studied the association thermodynamics and conformational stability of small β-sheet wild-type A$\beta_{17–42}$ oligomers with the different charge state of Glu^{22} and the Dutch (E22Q) mutants. We have found that the peptide charge reduction due to the mutation or the protonation of the solvent-exposed Glu^{22} results in a significant shift of the balance between the different physical components of the association free energy for all models. At the same time, the overall change in the association free energy for the E22Q mutants is relatively small, compared to the change of the individual components of the free energy (in this study no statistically significant difference was found between the association free energy for the wild-type oligomers at neutral pH and the E22Q mutants). This is a consequence of the complementarity and the resulting partial compensation between the direct (gas-phase) and the solvation electrostatic effects. Experimentally, the E22Q mutants demonstrate higher oligomerization propensity, compared to the wild-type case (35–39). There is also experimental evidence of similarities between the thermodynamics and kinetics of aggregation of A$\beta_{1–40}$ peptides; note also that at the higher aggregation rate, the Dutch A$\beta_{1–40}$ mutants may be thermodynamically more stable (13). Thus, our results suggest that the difference in the oligomerization propensity may be defined by the early stages of aggregation, namely, by the conversion of Aβ monomers from the random coil to the β-sheet conformation (17,18,21,24). It is worth mentioning that our simulations were restricted to the nanosecond timescale, whereas major conformational changes may occur in longer simulations with possible implications for the association thermodynamics.

The association free energy of the β-sheet wild-type A$\beta_{17–42}$ oligomers with Glu^{22} protonated at acidic conditions, is significantly lower, compared to both the wild-type oligomers at neutral pH and the Dutch mutants. Moreover, small oligomers with protonated Glu^{22} may become thermodynamically stable, which makes possible fibrilization

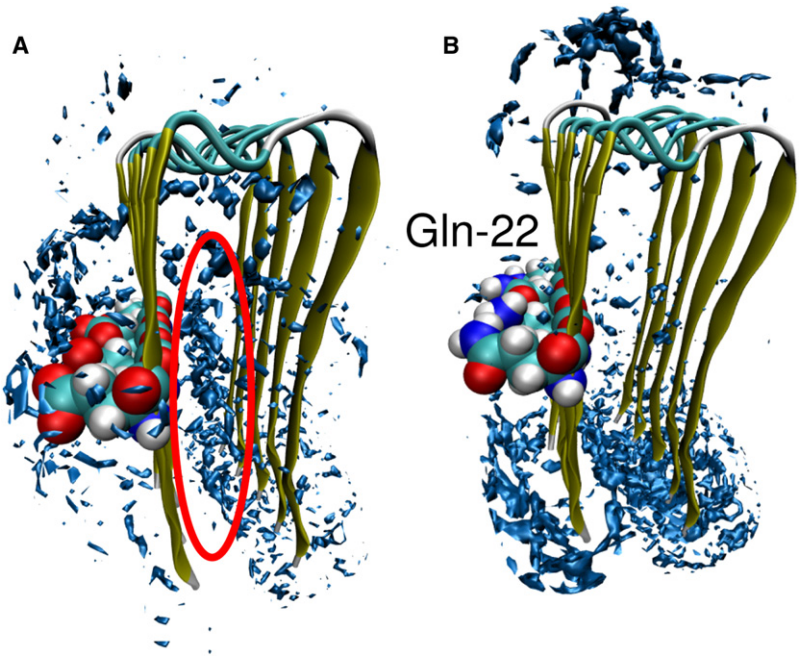

FIGURE 9 Effect of the Dutch mutation on the local entropic contribution to the solvation free energy. Results are for (*A*) the wild-type and (*B*) the Dutch mutant A$\beta_{17–42}$ pentamers. (*Left panel*, *red ellipse*) Contribution of the internal domains to the entropic part of the solvation free energy for the wild-type oligomer. Isosurfaces correspond to the local entropic contribution to the solvation free energy of 0.6 kcal/(mol Å^3) for the WT pH 7 model and 0.1 kcal/(mol Å^3) for the Dutch mutant. Image was produced with VMD (99).

through association of the preformed aggregates, in agreement with the experimental data (40). Lowering the association free energy is related not only to the reduction of the direct electrostatic interactions between peptides (which is largely offset by the increase in the solvation energetic penalty), but also to the change in the nonpolar energetics. The reason for that is twofold.

First, there is an increase in the favorable contribution of the dispersion interactions to the association free energy upon the protonation of Glu^{22} related to more optimal packing of the peptide side chains in the oligomers. This may be explained by destabilization of the (transient) inter- and intrapeptide salt bridges between Asp^{23} and Lys^{28}.

Secondly, the neutralization of the solvent-exposed side chains affects the microscopic solvation structure around the peptides. As a result, there is a change in the solvation entropic effects (hydrophobicity) related to the solvent organization, additionally to the changes introduced because of the differences in the conformational dynamics of the oligomers at different solvent conditions. Neutralization of peptides also eliminates the possibility of formation of water bridges at Glu^{22}, which may reduce the stability of the wild-type oligomers with protonated Glu^{22}.

In summary, for all oligomers the entropic contribution to the solvation free energy always favors their thermodynamic stability. The nonspecific dispersion interactions are another important factor contributing to the stabilization of the β-sheet oligomers. The latter is related to the high degree of the shape complementarity and tight packing of the Aβ peptides in the β-sheet oligomers. At the same time, our calculations revealed that the small wild-type $A\beta_{17-42}$ oligomers at neutral pH and the Dutch mutants with the pronounced β-sheet structure have positive association free energy. An implication is that in longer simulations (on timescales of microseconds and beyond), major structural changes may occur and oligomers may lose structural similarity with the mature amyloid fibril or dissociate, as observed in some experiments (94–96).

SUPPORTING MATERIAL

Four figures are available at http://www.biophysj.org/biophysj/supplemental/S0006-3495(09)01610-5.

The computations were supported by the Centre of Excellence in Integrated Nanotools at the University of Alberta.

We acknowledge financial support by the Alberta Prion Research Institute and the National Research Council of Canada.

REFERENCES

1. Caughey, B., and P. T. Lansbury. 2003. Protofibrils, pores, fibrils, and neurodegeneration: separating the responsible protein aggregates from the innocent bystanders. *Annu. Rev. Neurosci.* 26:267–298.
2. Prusiner, S. B. 1998. Prions. *Proc. Natl. Acad. Sci. USA.* 95:13363–13383.
3. Sunde, M., L. C. Serpell, …, C. C. Blake. 1997. Common core structure of amyloid fibrils by synchrotron x-ray diffraction. *J. Mol. Biol.* 273:729–739.
4. Nelson, R., M. R. Sawaya, …, D. Eisenberg. 2005. Structure of the cross-β spine of amyloid-like fibrils. *Nature.* 435:773–778.
5. Sawaya, M. R., S. Sambashivan, …, D. Eisenberg. 2007. Atomic structures of amyloid cross-β spines reveal varied steric zippers. *Nature.* 447:453–457.
6. Petkova, A. T., W.-M. Yau, and R. Tycko. 2006. Experimental constraints on quaternary structure in Alzheimer's β-amyloid fibrils. *Biochemistry.* 45:498–512.
7. Petkova, A. T., Y. Ishii, …, R. Tycko. 2002. A structural model for Alzheimer's β -amyloid fibrils based on experimental constraints from solid state NMR. *Proc. Natl. Acad. Sci. USA.* 99:16742–16747.
8. Lührs, T., C. Ritter, …, R. Riek. 2005. 3D structure of Alzheimer's amyloid-β(1–42) fibrils. *Proc. Natl. Acad. Sci. USA.* 102:17342–17347.
9. Teplow, D. B. 1998. Structural and kinetic features of amyloid beta-protein fibrillogenesis. *Amyloid.* 5:121–142.
10. Lansbury, Jr., P. T. 1999. Evolution of amyloid: what normal protein folding may tell us about fibrillogenesis and disease. *Proc. Natl. Acad. Sci. USA.* 96:3342–3344.
11. Knowles, T. P. J., W. Shu, …, M. E. Welland. 2007. Kinetics and thermodynamics of amyloid formation from direct measurements of fluctuations in fibril mass. *Proc. Natl. Acad. Sci. USA.* 104:10016–10021.
12. Jarrett, J. T., and P. T. Lansbury, Jr. 1993. Seeding "one-dimensional crystallization" of amyloid: a pathogenic mechanism in Alzheimer's disease and scrapie? *Cell.* 73:1055–1058.
13. Meinhardt, J., G. G. Tartaglia, …, M. Fändrich. 2007. Similarities in the thermodynamics and kinetics of aggregation of disease-related Aβ (1–40) peptides. *Protein Sci.* 16:1214–1222.
14. Kusumoto, Y., A. Lomakin, …, G. B. Benedek. 1998. Temperature dependence of amyloid β-protein fibrilization. *Proc. Natl. Acad. Sci. USA.* 95:12277–12282.
15. Auer, S., C. M. Dobson, and M. Vendruscolo. 2007. Characterization of the nucleation barriers for protein aggregation and amyloid formation. *HFSP J.* 1:137–146.
16. Hoang, T. X., A. Trovato, …, A. Maritan. 2004. Geometry and symmetry presculpt the free-energy landscape of proteins. *Proc. Natl. Acad. Sci. USA.* 101:7960–7964.
17. Lazo, N. D., M. A. Grant, …, D. B. Teplow. 2005. On the nucleation of amyloid β-protein monomer folding. *Protein Sci.* 14:1581–1596.
18. Cruz, L., B. Urbanc, …, H. E. Stanley. 2005. Solvent and mutation effects on the nucleation of amyloid β-protein folding. *Proc. Natl. Acad. Sci. USA.* 102:18258–18263.
19. Borreguero, J. M., B. Urbanc, …, H. E. Stanley. 2005. Folding events in the 21–30 region of amyloid β-protein (Aβ) studied in silico. *Proc. Natl. Acad. Sci. USA.* 102:6015–6020.
20. Urbanc, B., L. Cruz, …, H. E. Stanley. 2004. In silico study of amyloid β-protein folding and oligomerization. *Proc. Natl. Acad. Sci. USA.* 101:17345–17350.
21. Baumketner, A., M. G. Krone, and J.-E. Shea. 2008. Role of the familial Dutch mutation E22Q in the folding and aggregation of the 15–28 fragment of the Alzheimer amyloid-β protein. *Proc. Natl. Acad. Sci. USA.* 105:6027–6032.
22. Massi, F., D. Klimov, …, J. E. Straub. 2002. Charge states rather than propensity for β-structure determine enhanced fibrillogenesis in wild-type Alzheimer's β-amyloid peptide compared to E22Q Dutch mutant. *Protein Sci.* 11:1639–1647.
23. Massi, F., and J. E. Straub. 2001. Probing the origins of increased activity of the E22Q "Dutch" mutant Alzheimer's β-amyloid peptide. *Biophys. J.* 81:697–709.
24. Grant, M. A., N. D. Lazo, …, D. B. Teplow. 2007. Familial Alzheimer's disease mutations alter the stability of the amyloid β-protein monomer folding nucleus. *Proc. Natl. Acad. Sci. USA.* 104:16522–16527.

25. Zheng, J., H. Jang, …, R. Nussinov. 2007. Modeling the Alzheimer Aβ 17–42 fibril architecture: tight intermolecular sheet-sheet association and intramolecular hydrated cavities. *Biophys. J.* 93:3046–3057.
26. Buchete, N.-V., R. Tycko, and G. Hummer. 2005. Molecular dynamics simulations of Alzheimer's β-amyloid protofilaments. *J. Mol. Biol.* 353:804–821.
27. Buchete, N.-V., and G. Hummer. 2007. Structure and dynamics of parallel β-sheets, hydrophobic core, and loops in Alzheimer's Aβ fibrils. *Biophys. J.* 92:3032–3039.
28. Ma, B., and R. Nussinov. 2002. Stabilities and conformations of Alzheimer's β-amyloid peptide oligomers (Aβ 16–22, Aβ 16–35, and Aβ 10–35): sequence effects. *Proc. Natl. Acad. Sci. USA.* 99:14126–14131.
29. Ma, B., and R. Nussinov. 2002. Molecular dynamics simulations of alanine-rich β-sheet oligomers: insight into amyloid formation. *Protein Sci.* 11:2335–2350.
30. Fawzi, N. L., K. L. Kohlstedt, …, T. Head-Gordon. 2008. Protofibril assemblies of the arctic, Dutch, and Flemish mutants of the Alzheimer's Aβ1–40 peptide. *Biophys. J.* 94:2007–2016.
31. Takeda, T., and D. K. Klimov. 2008. Temperature-induced dissociation of Aβ monomers from amyloid fibril. *Biophys. J.* 95:1758–1772.
32. Shankar, G. M., S. Li, …, D. J. Selkoe. 2008. Amyloid-β protein dimers isolated directly from Alzheimer's brains impair synaptic plasticity and memory. *Nat. Med.* 14:837–842.
33. Van Broeckhoven, C., J. Haan, …, R. A. Roos. 1990. Amyloidβ protein precursor gene and hereditary cerebral hemorrhage with amyloidosis (Dutch). *Science.* 248:1120–1122.
34. Levy, E., M. D. Carman, …, B. Frangione. 1990. Mutation of the Alzheimer's disease amyloid gene in hereditary cerebral hemorrhage, Dutch type. *Science.* 248:1124–1126.
35. Esler, W. P., A. M. Felix, …, J. E. Maggio. 2000. Activation barriers to structural transition determine deposition rates of Alzheimer's disease Aβ amyloid. *J. Struct. Biol.* 130:174–183.
36. Sian, A. K., E. R. Frears, …, B. M. Austen. 2000. Oligomerization of β-amyloid of the Alzheimer's and the Dutch-cerebral-hemorrhage types. *Biochem. J.* 349:299–308.
37. Miravalle, L., T. Tokuda, …, J. Ghiso. 2000. Substitutions at codon 22 of Alzheimer's Aβ peptide induce diverse conformational changes and apoptotic effects in human cerebral endothelial cells. *J. Biol. Chem.* 275:27110–27116.
38. Watson, D. J., D. J. Selkoe, and D. B. Teplow. 1999. Effects of the amyloid precursor protein $Glu^{693} \rightarrow$Gln "Dutch" mutation on the production and stability of amyloid β-protein. *Biochem. J.* 340:703–709.
39. Watson, D. J., A. D. Lander, and D. J. Selkoe. 1997. Heparin-binding properties of the amyloidogenic peptides Aβ and amylin. Dependence on aggregation state and inhibition by Congo red. *J. Biol. Chem.* 272:31617–31624.
40. Carrotta, R., M. Manno, …, P. L. San Biagio. 2005. Protofibril formation of amyloid β-protein at low pH via a non-cooperative elongation mechanism. *J. Biol. Chem.* 280:30001–30008.
41. Karplus, M. 2002. Molecular dynamics simulations of biomolecules. *Acc. Chem. Res.* 35:321–323.
42. Huet, A., and P. Derreumaux. 2006. Impact of the mutation A21G (Flemish variant) on Alzheimer's β-amyloid dimers by molecular dynamics simulations. *Biophys. J.* 91:3829–3840.
43. Hills, Jr., R. D., and C. L. Brooks, 3rd. 2007. Hydrophobic cooperativity as a mechanism for amyloid nucleation. *J. Mol. Biol.* 368:894–901.
44. Hwang, W., S. Zhang, …, M. Karplus. 2004. Kinetic control of dimer structure formation in amyloid fibrillogenesis. *Proc. Natl. Acad. Sci. USA.* 101:12916–12921.
45. Nguyen, P. H., M. S. Li, …, D. Thirumalai. 2007. Monomer adds to preformed structured oligomers of Aβ-peptides by a two-stage dock-lock mechanism. *Proc. Natl. Acad. Sci. USA.* 104:111–116.
46. Dima, R. I., and D. Thirumalai. 2004. Probing the instabilities in the dynamics of helical fragments from mouse PrP^{C}. *Proc. Natl. Acad. Sci. USA.* 101:15335–15340.
47. DeMarco, M. L., and V. Daggett. 2007. Molecular mechanism for low pH triggered misfolding of the human prion protein. *Biochemistry.* 46:3045–3054.
48. DeMarco, M. L., and V. Daggett. 2004. From conversion to aggregation: protofibril formation of the prion protein. *Proc. Natl. Acad. Sci. USA.* 101:2293–2298.
49. Langella, E., R. Improta, and V. Barone. 2004. Checking the pH-induced conformational transition of prion protein by molecular dynamics simulations: effect of protonation of histidine residues. *Biophys. J.* 87:3623–3632.
50. De Simone, A., A. Zagari, and P. Derreumaux. 2007. Structural and hydration properties of the partially unfolded states of the prion protein. *Biophys. J.* 93:1284–1292.
51. Flöck, D., S. Colacino, …, A. D. Nola. 2006. Misfolding of the amyloid β-protein: a molecular dynamics study. *Proteins: Struct. Funct. Bioinform.* 62:183–192.
52. Tsai, H.-H. G., M. Reches, …, R. Nussinov. 2005. Energy landscape of amyloidogenic peptide oligomerization by parallel-tempering molecular dynamics simulation: significant role of Asn ladder. *Proc. Natl. Acad. Sci. USA.* 102:8174–8179.
53. Itoh, S. G., and Y. Okamoto. 2008. Amyloid-β(29–42) dimer formations studied by a multicanonical-multioverlap molecular dynamics simulation. *J. Phys. Chem. B.* 112:2767–2770.
54. Daidone, I., F. Simona, …, A. D. Nola. 2004. Beta-hairpin conformation of fibrillogenic peptides: structure and α-β transition mechanism revealed by molecular dynamics simulations. *Proteins: Struct. Funct. Bioinform.* 57:198–204.
55. Wei, G., N. Mousseau, and P. Derreumaux. 2007. Computational simulations of the early steps of protein aggregation. *Prion.* 1:3–8.
56. Hall, C. K., and V. A. Wagoner. 2006. Computational approaches to fibril structure and formation. *Methods Enzymol.* 412:338–365.
57. Röhrig, U. F., A. Laio, …, R. Petronzio. 2006. Stability and structure of oligomers of the Alzheimer peptide Aβ16–22: from the dimer to the 32-mer. *Biophys. J.* 91:3217–3229.
58. Wagoner, J. A., and N. A. Baker. 2006. Assessing implicit models for nonpolar mean solvation forces: the importance of dispersion and volume terms. *Proc. Natl. Acad. Sci. USA.* 103:8331–8336.
59. Levy, R. M., L. Y. Zhang, …, A. K. Felts. 2003. On the nonpolar hydration free energy of proteins: surface area and continuum solvent models for the solute-solvent interaction energy. *J. Am. Chem. Soc.* 125: 9523–9530.
60. Kovalenko, A. 2003. Three-dimensional RISM theory for molecular liquids and solid-liquid interfaces. *In* Molecular Theory of Solvation, Understanding Chemical Reactivity, Vol. 24. F. Hirata, editor. Kluwer Academic Publishers, Dordrecht.
61. Imai, T., S. Ohyama, …, F. Hirata. 2007. Theoretical study of the partial molar volume change associated with the pressure-induced structural transition of ubiquitin. *Protein Sci.* 16:1927–1933.
62. Imai, T., R. Hiraoka, …, F. Hirata. 2007. Locating missing water molecules in protein cavities by the three-dimensional reference interaction site model theory of molecular solvation. *Proteins: Struct. Funct. Bioinform.* 66:804–813.
63. Imai, T., R. Hiraoka, …, F. Hirata. 2007. Three-dimensional distribution function theory for the prediction of protein-ligand binding sites and affinities: application to the binding of noble gases to hen egg-white lysozyme in aqueous solution. *J. Phys. Chem. B.* 111: 11585–11591.
64. Imai, T., Y. Harano, …, F. Hirata. 2007. Theoretical analysis on changes in thermodynamic quantities upon protein folding: essential role of hydration. *J. Chem. Phys.* 126:225102.
65. Imai, T., Y. Harano, …, F. Hirata. 2006. A theoretical analysis on hydration thermodynamics of proteins. *J. Chem. Phys.* 125:024911.
66. Harano, Y., T. Imai, …, F. Hirata. 2001. Theoretical study for partial molar volume of amino acids and polypeptides by the three-dimensional reference interaction site model. *J. Chem. Phys.* 114: 9506–9511.

67. Drabik, P., S. Gusarov, and A. Kovalenko. 2007. Microtubule stability studied by three-dimensional molecular theory of solvation. *Biophys. J.* 92:394–403.

68. Imai, T., H. Isogai, …, F. Hirata. 2006. Theoretical study of volume changes accompanying xenon-lysozyme binding: implications for the molecular mechanism of pressure reversal of anesthesia. *J. Phys. Chem. B.* 110:12149–12154.

69. Imai, T., A. Kovalenko, and F. Hirata. 2006. Hydration structure, thermodynamics, and functions of protein studied by the 3D-RISM theory. *Mol. Simul.* 32:817–824.

70. Imai, T., R. Hiraoka, …, F. Hirata. 2005. Water molecules in a protein cavity detected by a statistical-mechanical theory. *J. Am. Chem. Soc.* 127:15334–15335.

71. Lazaridis, T., and M. Karplus. 1999. Effective energy function for proteins in solution. *Proteins: Struct. Funct. Gen.* 35:133–152.

72. Christopher, M., M. K. Dobson, and A. Scaronali. 1998. Protein folding: a perspective from theory and experiment. *Angew. Chem. Int. Ed.* 37:868–893.

73. Srinivasan, J., T. Cheatham, …, D. Case. 1998. Continuum solvent studies of the stability of DNA, RNA, and phosphoramidate-DNA helices. *J. Am. Chem. Soc.* 120:9401–9409.

74. Gohlke, H., and D. A. Case. 2004. Converging free energy estimates: MM-PB(GB)SA studies on the protein-protein complex Ras-Raf. *J. Comput. Chem.* 25:238–250.

75. Massova, I., and P. Kollman. 1999. Computational alanine scanning to probe protein-protein interactions: a novel approach to evaluate binding free energies. *J. Am. Chem. Soc.* 121:8133–8143.

76. Lee, M. R., Y. Duan, and P. A. Kollman. 2000. Use of MM-PB/SA in estimating the free energies of proteins: application to native, intermediates, and unfolded villin headpiece. *Proteins: Struct. Funct. Gen.* 39:309–316.

77. Case, D. A., T. E. Cheatham, 3rd, …, R. J. Woods. 2005. The AMBER biomolecular simulation programs. *J. Comput. Chem.* 26:1668–1688.

78. Ding, F., J. J. LaRocque, and N. V. Dokholyan. 2005. Direct observation of protein folding, aggregation, and a prion-like conformational conversion. *J. Biol. Chem.* 280:40235–40240.

79. Lum, K., D. Chandler, and J. Weeks. 1999. Hydrophobicity at small and large length scales. *J. Phys. Chem. B.* 103:4570–4577.

80. Luchko, T, S. Gusarov, …, A. Kovalenko. 2009. Three-dimensional molecular theory of solvation coupled with molecular dynamics in amber. *J. Chem. Theory Comput.* In press.

81. Wang, L., Y. Duan, …, P. A. Kollman. 1999. Study of the stability and unfolding mechanism of BBA1 by molecular dynamics simulations at different temperatures. *Protein Sci.* 8:1292–1304.

82. Hui Li, J. H. J., and Andrew D. Robertson. 2005. Very fast empirical prediction and rationalization of protein pKa values. *Proteins: Struct. Funct. Bioinform.* 61:704–721.

83. Berendsen, H. J. C., J. R. Grigera, and T. P. Straatsma. 1987. The missing term in effective pair potentials. *J. Phys. Chem.* 91:6269–6271.

84. Allen, M. P., and D. J. Tildesley. 1989. Computer Simulation of Liquids. Clarendon Press, New York.

85. Hansen, J. P., and I. R. McDonald. 1986. Theory of Simple Liquids. Academic Press, London.

86. Chandler, D., and H. C. Andersen. 1972. Optimized cluster expansions for classical fluids. II. Theory of molecular liquids. *J. Chem. Phys.* 57:1930–1937.

87. Hirata, F. 2003. Theory of molecular Liquids. *In* Molecular Theory of Solvation, Understanding Chemical Reactivity, Vol. 24 F. Hirata, editor. Kluwer Academic Publishers, Dordrecht.

88. Beglov, D., and B. Roux. 1997. An integral equation to describe the solvation of polar molecules in liquid water. *J. Phys. Chem. B.* 101:7821–7826.

89. Kovalenko, A., and F. Hirata. 1999. Self-consistent description of a metal-water interface by the Kohn-Sham density functional theory and the three-dimensional reference interaction site model. *J. Chem. Phys.* 110:10095–10112.

90. Miyata, T., and F. Hirata. 2007. Combination of molecular dynamics method and 3D-RISM theory for conformational sampling of large flexible molecules in solution. *J. Comput. Chem.* 29:871–882.

91. Smith, D. E., and A. D. J. Haymet. 1993. Free energy, entropy, and internal energy of hydrophobic interactions: computer simulations. *J. Chem. Phys.* 98:6445–6454.

92. Duan, Y., and P. A. Kollman. 1998. Pathways to a protein folding intermediate observed in a 1-microsecond simulation in aqueous solution. *Science.* 282:740–744.

93. Garzon-Rodriguez, W., M. Sepulveda-Becerra, …, C. G. Glabe. 1997. Soluble amyloid Aβ-(1–40) exists as a stable dimer at low concentrations. *J. Biol. Chem.* 272:21037–21044.

94. Kayed, R., E. Head, …, C. G. Glabe. 2003. Common structure of soluble amyloid oligomers implies common mechanism of pathogenesis. *Science.* 300:486–489.

95. Hou, L., H. Shao, …, M. G. Zagorski. 2004. Solution NMR studies of the A β(1–40) and A β(1–42) peptides establish that the Met^{35} oxidation state affects the mechanism of amyloid formation. *J. Am. Chem. Soc.* 126:1992–2005.

96. Hou, L., I. Kang, …, M. G. Zagorski. 2002. Methionine 35 oxidation reduces fibril assembly of the amyloid Aβ-(1–42) peptide of Alzheimer's disease. *J. Biol. Chem.* 277:40173–40176.

97. Guest, W., N. Cashman, and S. Plotkin. An estimate of PrPc β sheet dissociation Gibbs free energy: implications for prion conversion. *Prion 2008 Conference, Oct 8–10, 2008; Madrid.*

98. Klug, G. M. J. A., D. Losic, …, D. H. Small. 2003. Beta-amyloid protein oligomers induced by metal ions and acid pH are distinct from those generated by slow spontaneous ageing at neutral pH. *Eur. J. Biochem.* 270:4282–4293.

99. Humphrey, W., A. Dalke, and K. Schulten. 1996. VMD—visual molecular dynamics. *J. Mol. Graph.* 14:33–38, 27–28.